Cellular and Molecular Life Sciences (2024) 81:19
https://doi.org/10.1007/s00018-023-05051-9

ORIGINAL ARTICLE

Calcium-sensing receptor and NF-κB pathways in TN breast cancer contribute to cancer-induced cardiomyocyte damage via activating neutrophil extracellular traps formation

Jingya Zeng[1] · Yangyang Cheng[1] · Wanlin Xie[1] · Xin Lin[1] · Chenglong Ding[2] · Huimin Xu[1] · Baohong Cui[1] · Yixin Chen[1] · Song Gao[1] · Siwen Zhang[1] · Kaiyue Liu[1] · Yue Lu[1] · Jialing Zhou[1] · Zhongxiang Shi[1] · Yihua Sun[1]

Received: 18 August 2023 / Revised: 26 October 2023 / Accepted: 28 October 2023

Abstract

Cardiovascular disorders are commonly prevalent in cancer patients, yet the mechanistic link between them remains poorly understood. Because neutrophil extracellular traps (NETs) have implications not just in cardiovascular diseases (CVD), but also in breast cancer (BC), it was hypothesized to contribute to CVD in the context of oncogenesis. We established a mouse model using nude mice to simulate liver metastasis of triple-negative BC (TNBC) through the injection of MDA-MB-231 cells. Multiple imaging and analysis techniques were employed to assess the cardiac function and structure, including echocardiography, HE staining, Masson staining, and transmission electron microscopy (TEM). MDA-MB-231 cells underwent treatment with a CaSR inhibitor, CaSR agonist, and NF-κB channel blocker. The phosphorylation of NF-κB channel protein p65 and the expression and secretion of IL-8 were assessed using qRT-PCR, Western Blot, and ELISA, respectively. In addition, MDA-MB-231 cells were co-cultured with polymorphonuclear neutrophils (PMN) under varying conditions. The co-localization of PMN extracellular myeloperoxidase (MPO) and DNA were observed by cellular immunofluorescence staining to identify the formation of NETs. Then, the cardiomyocytes were co-cultured with the above medium that contains NETs or not, respectively; the effects of NETs on cardiomyocytes apoptosis were perceived by flow cytometry. The ultrastructural changes of myocardial cells were perceived by TEM, and ELISA detected the levels of myocardial enzyme (LDH, MDA and SOD). Overall, according to our research, CaSR has been found to have a regulatory role in IL-8 secretion in MDA-MB-231 cells, as well as in the formation of NETs by PMN cells. These findings suggest CaSR-mediated stimulation in PMN can lead to increased NETs formation and subsequently to cytotoxicity in cardiomyocytes, which potentially via activation of the NF-κB signaling cascade of BC cell.

Keywords TNbreast cancer · Calcium-sensing receptor · Neutrophil extracellular traps · Myocardial injury · NF-κB signaling pathway

Abbreviations

BC	Breast cancer
CaSR	Calcium-sensing receptor
Cit H_3	Citrullinated histone H_3
CVD	Cardiovascular diseases
G-CSF	Granulocyte colony-stimulating factor
H_2O_2	Hydrogen peroxide
IL	Interleukin
LPS	Lipopolysaccharides
MPO	Myeloperoxidase
NE	Neutrophil elastase
NETs	Neutrophil extracellular traps
NF-κB	Nuclear factor kappaB
PMA	Phorbol-12-myristate-13-acetate
PMN	Polymorphonuclear neutrophils
TNF	Tumor necrosis factor

Co-first author: Jingya Zeng and Yangyang Cheng.

✉ Yihua Sun
600611@hrbmu.edu.cn

[1] Department of Clinical Laboratory, Harbin Medical University Cancer Hospital, Harbin 150081, Heilongjiang, China

[2] Department of Pathology, The First Affiliated Hospital of Jiamusi University, Jiamusi 154003, Heilongjiang, China

Published online: 10 January 2024

Introduction

The impact of environmental aspects on the occurrence and progression of cancer is widely accepted in the medical community. Known factors include exposure to chemical pollutants, contaminated air and water, dietary and lifestyle choices, and occupational hazards. Recently, clinical data suggest that cardiovascular diseases (CVD) are now a leading cause of death among individuals who have survived cancer.

The discipline of cardio-oncology, however, is in its early stages with initial research focusing primarily on the side-effects of chemotherapy and radiotherapy.

Breast cancer (BC) poses a significant global healthcare challenge due to its widespread prevalence and associated complications, such as metastasis and systemic effects. BC is notorious for its dual status as both the most prevalent malignant condition and the primary contributor to global cancer-related mortality [1]. Remarkable advancements in treatment strategies have led to an approximately 40% decline in BC mortality over the past four decades [2]. Nevertheless, a recent study involving 1.2 million BC patients revealed that the likelihood of mortality resulting from CVD surpassed that of cancer recurrence by a significant margin [3]. Thus, CVD has emerged as the primary factor contributing to mortality among individuals who have survived BC [4] and have the potential to limit subsequent treatment opportunities [5]. Consequently, it is imperative to promptly comprehend the mechanisms that lead to concurrent development of BC and CVD, with the ultimate goal of prolonging and enhancing the quality of life for BC survivors.

Previously, tumor-associated inflammation has been considered a hallmark of malignant tumors and is a critical factor in both the development and prognosis of cancer patients [6]. Inflammatory responses coincide with elevated biomarker levels, including TNF-α, CRP, IL-6, IL-10, IL-8, polymorphonuclear neutrophils (PMN), and thrombocytes, whereas levels of albumin and lymphocyte counts were found to be decreased [7–13]. Numerous studies have highlighted common risk factors between BC and CVD, such as chronic inflammation and oxidative stress, with PMN playing a critical role [14, 15].

PMN are known for creating neutrophil extracellular traps (NETs) consisting of various enzymes and cytokines [16, 17]. These NETs, consist of extracellular DNA wrapped in histones as well as accompanied by granular proteases, are created in response to diverse pathogens, such as bacteria, fungi, viruses, and protozoa [16]. Host factors such as activated platelets, inflammatory stimuli, and certain chemical compounds can trigger the formation of NETs, which are critical in localizing and neutralizing pathogens [18]. NETs are now recognized to form even in sterile inflammation conditions, including CVD, cancer, and autoimmunity [19–21]. Researchers have documented a higher propensity in tumor-bearing mice to generate NETs as compared to healthy specimens [22]. Elevated levels of NETs have been found in individuals having advanced-stage tumors as compared to localized ones. Notably, NET formation showed a strong correlation with the progression of BC [23].

The calcium-sensing receptor (CaSR), belongs to the superfamily of G protein-coupled receptors, is widely distributed in a series of tissues as well as cells and regulates several cellular processes, including gene expression, secretion, differentiation, proliferation, apoptosis, and more [24–26]. There is growing evidence that aberrant activation and expression of the CaSR occur in malignant tumor tissues [27–29]. An increment in CaSR gene mutations has been observed in BC tissues as compared to benign breast lesions, and these mutation levels positively correlate with the prognosis and metastatic potential of BC [30]. The role of CaSR in promoting the secretion of cytokines and mitigating PMN-induced harm through the NF-κB and MAPKs signaling pathways has also been reported by our team [31–33].

Activated PMN release NETs under the influence of various substances including pathogens, activated platelets, PMA, LPS, IL-8, G-CSF, and TNF-α, whose concentrations are also altered in the microenvironment of BC [34]. The question that remains is whether CaSR regulates secretion from BC cells to stimulate PMN to form NETs and subsequently contribute to cardiac injury.

The investigation of CVD in cancer patients is just beginning, with the current focus primarily on treatment resistance and side-effects. The role of peripheral blood cells in this context has been under-investigated despite its potential therapeutic impact. This study aims to shed light on the intricacies of CaSR, cytokines, and NETs' relationship in BC-induced myocardial injury with the hope of identifying new therapeutic targets for preventing and treating CVD in cancer patients.

Materials and methods

Cell culture

MCF7 and MDA-MB-231, two human BC cell lines, specifically an estrogen receptor-positive subtype and a TNBC subtype, respectively, were acquired from the Cell Bank of the Chinese Academy of Sciences. The MCF7 cells were cultured in MEM medium, with 10% FBS and 1% penicillin – streptomycin, all from different suppliers (Gibco, USA for MEM medium, BI, Israel for FBS, and Beyotime, China for penicillin – streptomycin). In contrast, the MDA-MB-231

cells were cultured applying L-15 medium obtained from Gibco, which was supplemented with an equivalent concentration of FBS, penicillin, and streptomycin. Cells were cultured under similar conditions of 37 °C in a humidified atmosphere with 5% CO_2.

Primary cardiomyocytes cultures

Neonatal ventricular myocytes were obtained from a single Kunming mouse aged 2–3 days old, which was sourced from the Animal Research Institute at Harbin Medical University, following a previously established protocol [35]. Initially, the hearts were dissected and minced into small fragments, which were then subjected to digestion using a combination of 0.5% trypsinase and 0.1% type I collagenase (supplied by Beyotime, China) at 37 °C for 10 min. The enzymatic digestion was halted by adding DMEM culture medium (obtained from Gibco, USA). The resulting cell suspension underwent centrifugation at 800 × g at 4 °C for 20 min, and the resulting pellet was subsequently resuspended in DMEM. This cellular suspension was then incubated in the culture condition for 2 h. During this incubation period, nonadherent cardiomyocytes were effectively separated from the adherent cells. The nonadherent cardiomyocytes were then cultured in a petri dish coated with collagen, with the addition of 10% FBS as well as 1% penicillin – streptomycin. The culture medium was refreshed periodically, every 2–3 days, to ensure the continuous viability and growth of the cells.

Isolation of neutrophils

Fresh whole-blood anticoagulated with EDTA was collected. Human neutrophil was isolated using polymorphprep™ (Axis-Shield, Norway). Briefly, an equal volume of a total of 5 ml of fresh whole blood was layered onto an equal volume of Polymorphprep in a 15 ml centrifuge tube. Next, the tube was subjected to centrifugation at room temperature (RT) for 30 min at a speed of 500 × g [36]. Subsequently, the lower leukocyte band, which was specifically enriched with neutrophils, was washed and subsequently resuspended in 5 ml of ACK lysis buffer, which was supplied by Beyotime, China. After undergoing two additional wash steps using HBSS without Ca_2^+/Mg_2^+, the neutrophils were ultimately resuspended in serum-free RPMI-1640 medium (obtained from Gibco, USA).

Inducing and suppressing the formation of NETs

According to our continuous experimental exploration, after isolating neutrophils from healthy controls, they were stimulated by incubation with 25 nM Phorbol 12-myristate 13-acetate (PMA) for a duration of 4 h. (purchased from MCE, USA). In the suppressing assay, a combination of PMA as well as inhibitors was used. After the 4-h PMA stimulation, DNase-1 at a concentration of 1 U/ml (obtained from Sigma, USA) was utilized to digest NETs scaffolds. The supernatants, which contained the NETs structures, were obtained by centrifuging the mixture at a speed of 250 × g for a duration of 10 min and stored at 4 °C until further analysis [37].

Immunofluorescence

NETs formation in vitro was assessed by seeding PMN cells onto poly-L-lysine-coated coverslips (Corning, USA). Following a 4-h stimulation with PMA, the cells were treated by fixing them with 4% paraformaldehyde at room temperature for a duration of 10 min. Subsequently, PBS was employed for rinsing, followed by incubation in a 50 mM NH_4Cl solution for another 10 min. Permeabilization of the cells was achieved using 0.5% Triton X-100 (ThermoFisher Scientific, USA) for 1 min at RT. Subsequently, the cells were blocked with a solution of PBS containing 1% bovine serum albumin (BSA) (Sigma, USA) for 30 min at 37 °C, and then incubated with an MPO antibody (Abcam, USA) diluted 1:400 in the blocking buffer for 1 h at RT. Following three washes with PBS, the cells were incubated with Alexa Fluor 594 (dilution of 1:200, Invitrogen, USA), a fluorochrome-conjugated secondary antibody, for 1 h at RT. The coverslips were rinsed in PBS, stained with DAPI (Beyotime, China) for 5 min, rinsed again, and mounted onto glass slides. Examination was performed with the aid of a fluorescence microscope (Leica, Germany), and the NETs were ascertained by calculating the ratio of neutrophils releasing NETs to the total amount of neutrophils.

Assessment of NETs formation

Indicators of NETs in the cellular culture supernatant included the presence of MPO – DNA complex, citrullinated histone H3 (Cit H_3), as well as neutrophil elastase (NE). Cit H_3 levels were determined by employing a selective ELISA kit (Cayman, USA) according to the provided instructions. NE levels were quantified using another selective ELISA kit (Cloud-Clone Corp, USA) following their respective instructions. The MPO – DNA complex was quantified using a capture ELISA method. In detail, 96-well plates were coated with 5 μg/mL anti-MPO antibody (Santa Cruz, USA), diluted 1:500 in 50 μL, and incubated overnight at 4 ℃. After three washes with 300 μL each, 20 μL of the samples were added and incubated for 80 μL. Following a 20-min incubation in the dark at room temperature (RT), the measurement of absorbance was performed at a wavelength of 405 nm. The formation of soluble NETs was quantified as the percentage increase in absorbance in relation to the control. The buffer utilized consisted of a peroxidase-labeled

anti-DNA monoclonal antibody (dilution 1:25, Cell Death ELISAplus, Roche, Switzerland). Following that, the plate was subjected to a 2-h incubation period at room temperature with continuous shaking at 300 rpm. After three washes using 300 µL each, 100 µL of peroxidase substrate (Beyotime, China) was introduced.

In vivo study

Female athymic BALB/c nude mice, aged 5–6 weeks and weighing 20–25 g, were obtained from Beijing Vital River Laboratory Animal Technology Co., Ltd (Beijing, China). These mice were subsequently housed at the Animal Reproduction Facility within the Department of Harbin Medical University. For the induction of experimental liver metastases, 1 × 106 MDA-MB-231 BC cells were intrasplenically injected using a 50 µL PBS suspension. The sham group received an intrasplenic injection of 50 µL PBS only. Following the injection of MDA-MB-231 BC cells, the treatment groups received intraperitoneal administration of DNase-1 at a dosage of 15,000 U/kg. On the other hand, the sham mice were treated with a solution of 0.1% DMSO in 100 µL saline. Euthanasia of the mice occurred during the 3rd, 5th, and 8th weeks subsequent to the initial injection. A total of 120 female athymic BALB/c nude mice were finally used in this study.

Western blot

Cell lysates were acquired by incubating cells in RIPA lysis buffer (Beyotime, China) supplemented with a kind of protease inhibitor (Roche, Switzerland) for 30 min. Bradford protein assay, with BSA as the standard, was employed to determine the protein concentration. Following that, 20 µg of the protein samples underwent loading onto a 10% SDS-PAGE gel and were subsequently transferred to a polyvinylidene fluoride membrane at 20 V for 20 min. Next, the membranes were blocked in 5% (w/v) skimmed milk in TBS-T at 37 ℃ for 1 h. Primary antibodies, namely anti-CaSR (1:500, Santa Cruz, USA), anti-P-p65 (1:1000, CST, USA), anti-p65 (1:1000, CST, USA), anti-IL-8 (1:1000, Wanleibio, China), and anti-GAPDH (1:1000, Wanleibio, China), were incubated with the membranes overnight at 4 ℃. Subsequently, a secondary antibody (dilution: 1:5000, ZSGB-BIO, China) was employed on the membrane. The signals were detected using the ECL kit (HaiGene, Harbin, China) and the Multiplex Fluorescent Imaging System (ProteinSimple, California, USA). Protein band intensities were quantified with the aid of a Bio-Rad ChemiDocTM EQ densitometer and Bio-Rad Quantity One software (Bio-Rad Laboratories, Hercules, CA, USA).

Animal echocardiography

The animals received 3% pentobarbital sodium for anesthesia. Subsequently, standard two-dimensional echocardiographic parameters of the left ventricle were captured using parasternal short-axis and long-axis views. The echocardiographic settings were meticulously optimized to enhance the signal-to-noise ratio and achieve precise endocardial delineation in the two-dimensional images.

Serum and tissue preparation

After an overnight fasting period, the animals were anesthetized using pentobarbital sodium to facilitate the collection of both blood and tissue samples. EDTA was added as an anticoagulant to the tubes used for blood sample collection. Subsequently, following careful dissection of the heart from its surrounding tissues, it was subsequently divided into three distinct sections. For the first portion of tissue samples, a 4% polyformaldehyde fixative was applied, followed by embedding in paraffin and dehydration using a sucrose gradient. The prepared samples were then subjected to various staining techniques including hematoxylin – eosin (H&E) staining, Masson staining, immunohistochemical staining, and immunofluorescent staining. Another portion of the tissues was fixed with a 2.5% glutaraldehyde solution to facilitate observation using a transmission electron microscope. Finally, the remaining samples were stored at – 80 ℃ for subsequent experimental purposes.

Analysis of the cardiomyocytes' ultrastructure utilizing a transmission electron microscope (TEM)

To investigate the ultrastructure of cardiomyocytes, heart tissues or primary cultured neonatal cardiomyocytes were fixed with a solution comprising 2.5% glutaraldehyde and subsequently treated with 1% osmium tetroxide. Subsequently, the tissues underwent a dehydration process utilizing a series of alcohols before being embedded. Finally, ultrathin slices measuring 50–70 µm were prepared. These sliced sections were then utilized for the observation of any ultrastructural modifications in cardiomyocytes using a transmission electron microscope (TEM).

Quantitative real-time PCR analysis

Both animal and cell samples were processed for qRT-PCR analysis using a cDNA kit (Roche, Switzerland) according to the provided guidelines. The qRT-PCR was carried out on a Roche LightCycler 96 instrument with the application of SYBR Green qPCR Master Mix. The reverse transcription step involved incubation at 95 °C for 10 min, followed by

a subsequent hour-long incubation at 42 °C. For the subsequent qPCR amplification, a Real-Time reaction mixture of 5 µl was prepared in a total volume of 50 µl. This reaction mixture contained customized gene-specific primers designed for the specific target sequences. The qPCR amplification consisted of a total of 40 cycles, involving denaturation at 95 °C for 15 s, followed by annealing at 56 °C for 60 s. Primers:

CaSR: 5′-GTCCAGAAGTCCCTCCCATC-3′ (forward), 5′-AACCACGCTTTCCTACCCTA-3′ (reverse);

IL-8: 5′-TAGCAAAATTGAGGCCAAGG-3′ (forward), 5′-AAACCAAGGCACAGTGGAAC-3′ (reverse);

GAPDH: 5′-GACATGCCGCCTGGAGAAAC-3′ (forward),

5′-AGCCCAGGATGCCCTTTAGT-3′ (reverse).

Immunohistochemistry

The samples underwent fixation in formalin, followed by subsequent paraffin embedding and sectioning into slices measuring 4 µm in thickness. These sections were then carefully mounted onto slides coated with silane. Antigen retrieval was performed by subjecting the samples to high-pressure conditions using EDTA (pH 8.0) for a duration of 2.5 min. Following the retrieval step, the sections were incubated overnight at 4 °C with specific primary antibodies: anti-Bax (1:400, CST, USA), anti-Bcl-2 (1:400, CST, USA), and anti-CaSR (1:50, Santa Cruz, USA). After a series of PBS washes, the sections were incubated with biotinylated IgG secondary antibody from ZSGB-BIO (China). The visualization of staining was achieved using 3,3′-diaminobenzidine (DAB) solution. Negative controls were incorporated by substituting the primary antibody with PBS to ensure specificity. The evaluation of tumor cells stained positively included the determination of the percentage of positive cells ranging from 0 to 100, and the categorization of staining intensity as 0 (on behalf of none), 1 (on behalf of mild), 2 (on behalf of moderate), or 3 (on behalf of strong), following well-established methodologies [38].

Protein chip technology

Utilizing the human cytokine array kit (R&D Systems, #ARY005B) and following the manufacturer's protocol, protein chip technology assays were conducted. Initially, culture supernatants were collected and subjected to centrifugation at 13,000 rpm for 10 min to remove debris. Following precoating with capture antibodies, the array membranes were incubated with 0.5 ml of culture supernatants overnight at 4 ℃. Subsequently, the membranes were subjected to three washes using 50 ml of washing buffer at room temperature, followed by incubation with a streptavidin – horseradish peroxidase-coupled antibody (diluted at 1:2000) for 30 min at room temperature (RT). The immunoblot images were captured and visualized using the ChemiDoc Imaging System (Bio-Rad), followed by quantification of spot intensity using ImageJ software. For cytokine level measurement, two spots per membrane were used, and their intensity mean was compared to the intensity mean of three internal controls on the same membrane. By calculating the ratio of specific intensity mean to control intensity mean, variations in hybridization efficiency across different experiments were accounted for.

Immunofluorescence in tissues

To visualize and detect NETs through immunofluorescence, the staining procedure outlined in reference [39] was implemented. Nonspecific binding sites were blocked by employing a solution of 2% goat serum in 2% BSA-PBS. Immunostaining was conducted using a rabbit anti-Cit H_3 polyclonal antibody (diluted 1:400, Abcam, USA) and a mouse anti-MPO monoclonal antibody (diluted 1:400, Santa Cruz, USA) as primary antibodies. Visualization of the staining was achieved by utilizing secondary antibodies conjugated with fluorochromes, while DAPI served as the counterstain for the sections. Capturing of images was performed using a laser scanning confocal microscope (LSCM; Olympus Co. Ltd., Tokyo, Japan). The presence of NETs was determined by the co-localization of DNA, MPO, and Cit H_3.

Apoptosis detection using flow cytometry

To assess the apoptotic ratio, flow cytometric analysis was conducted. After washing with an appropriate buffer, cardiomyocytes were exposed to 5 µl of Annexin V and 5 µl of PI for 15 min at room temperature. The apoptotic ratio was then quantified using flow cytometry (BD FACSCanto II; BD Biosciences, Franklin Lakes, NJ, USA) as the selected detection technique.

Detection of levels of myocardial enzyme and IL-8 by ELISA

We employed ELISA to analyze the levels of injury markers in cardiomyocytes under different experimental conditions, following the guidelines provided by the manufacturer (Beyotime, China).

Statistical analysis

GraphPad Prism 8.0 software was utilized for data mapping and curve fitting. SPSS 19.0 software was employed for statistical analyses. For comparisons involving three or more groups, one-way analysis of variance (ANOVA) followed by

the Student – Newman – Keuls test was employed. Meanwhile, the Student's *t* test was used to evaluate significant differences between two groups. A threshold of $p < 0.05$ was deemed statistically significant. The data were presented with the form of means ± SEM.

Results

Changes of NETs levels in liver metastasis-TNBC nude mice

To investigate the potential link between cancer and CVD, we developed liver metastasis models in nude mice through the injection of MDA-MB-231 cells, which have been reported to produce more NETs [40]. After performing HE staining, we observed the presence of metastatic BC nests in the liver tissue, confirming the successful construction of our model (see Fig. 1A). Samples were collected at 3, 5, and 8 weeks from both sham mice and model mice who were injected with MDA-MB-231 cells and/or NETs digestant DNase-1. We observed an increasing trend in the levels of NETs markers (MPO-DNA complex, Cit H_3, NE) in serum as time progressed in the nude mice. However, the administration of DNase-1 significantly decreased the levels of NETs in each group (see Fig. 1B–D). Co-localization of MPO, Cit H_3, and DNA in myocardial tissue was scarcely observed in the first three weeks, indicating the absence of NETs distribution. However, co-localization of MPO, Cit H_3, and DNA was evident in the myocardial tissue at the 5th and 8th weeks, with a higher distribution density observed in the 8th week compared to the 5th week. DNase-1 effectively reduced the distribution of NETs (see Fig. 1E). The expression pattern of Cit H_3 protein in myocardial tissue samples exhibited a similar trend to the distribution of NETs (see Fig. 1F).

Changes of heart function and cardiac markers in liver metastasis-TNBC nude mice

Echocardiography performed at the 8th week after the injection of MDA-MB-231 cells revealed significant impairment in cardiac function. This was indicated by a decrease in left ventricular ejection fraction (EF%) and fractional shortening (FS%), along with an elevation in the E/A ratio, isovolumic relaxation time (IVRT), and the ratio of the sum of ventricular isovolumic contraction time and ventricular diastolic contraction time to ejection time (Tei index) (see Fig. 2, panels A–C; Table 1).

LDH and MDA are indicators of cellular damage, while SOD is used to assess the antioxidant capacity of cells. By analyzing changes in these myocardial enzyme indices in the serum of nude mice, no significant disparity in myocardial enzyme levels was observed within the initial three weeks. However, at both the 5th and 8th weeks, there was an elevation in LDH and MDA levels, accompanied by a decrease in SOD levels. Notably, the changes observed in the 8th week were more pronounced compared to the 5th week. Injection of DNase-1 partially reversed these changes (see Table 2).

Expressions of the pro-apoptotic protein Bax as well as the anti-apoptotic protein Bcl-2 in myocardial tissue samples were evaluated through immunohistochemical staining (IHC). Initially, there were no marked variations in the expressions of Bcl-2 as well as Bax during the first three weeks. However, as time progressed, Bax expression increased while Bcl-2 levels gradually declined. Injection of DNase-1 partially reversed these results (see Fig. 2D–E).

Regarding changes in myocardial tissue structure, we observed that the myocardial tissue in the sham group and the 3rd week group appeared normal based on HE staining, Transmission Electron Microscope (TEM), and Masson staining evaluation. However, by the 5th week, the myocardial tissue structure showed apparent disorder with abnormal collagen deposition. Moreover, the ultrastructure of the myocardial tissue revealed fiber fracture, cavity formation, and degenerative necrosis, which became more pronounced in the 8th week. Injection of DNase-1 partially mitigated these changes (see Fig. 3A–C). Thus, these findings indicate that the degree of myocardial injury worsened with the progression of metastasis, and DNase-1 administration could reduce the severity of myocardial injury.

MDA-MB-231 cells stimulated PMN to form NETs

In order to investigate the factors contributing to the observed elevation of NETs in patients with TNBC, co-cultures were established for a duration of 4 h, involving either nontriple-negative BC MCF7 cells or TNBC MDA-MB-231 cells with polymorphonuclear leukocytes (PMN) (see Fig. 4, panel A). To assess the formation of NETs, PMN stimulated with PMA served as the positive control, while DNase-1 was used to degrade NETs. The levels of NETs markers and the co-localization of myeloperoxidase (MPO) and extracellular DNA were significantly elevated after PMA-induced PMN stimulation. Furthermore, we observed that only PMN co-cultured with MDA-MB-231 cells exhibited these changes, whereas MCF7 cells did not. The elevated indices were effectively reduced by the application of DNase-1 (see Fig. 4, panels B–E).

The concentration of IL-8 in BC was measured

In order to identify the key substance responsible for stimulating polymorphonuclear leukocytes (PMN) to form NETs in BC, protein chip technology was utilized to analyze the cytokines present in the supernatants of different groups, namely nontriple-negative BC cells (MCF7)

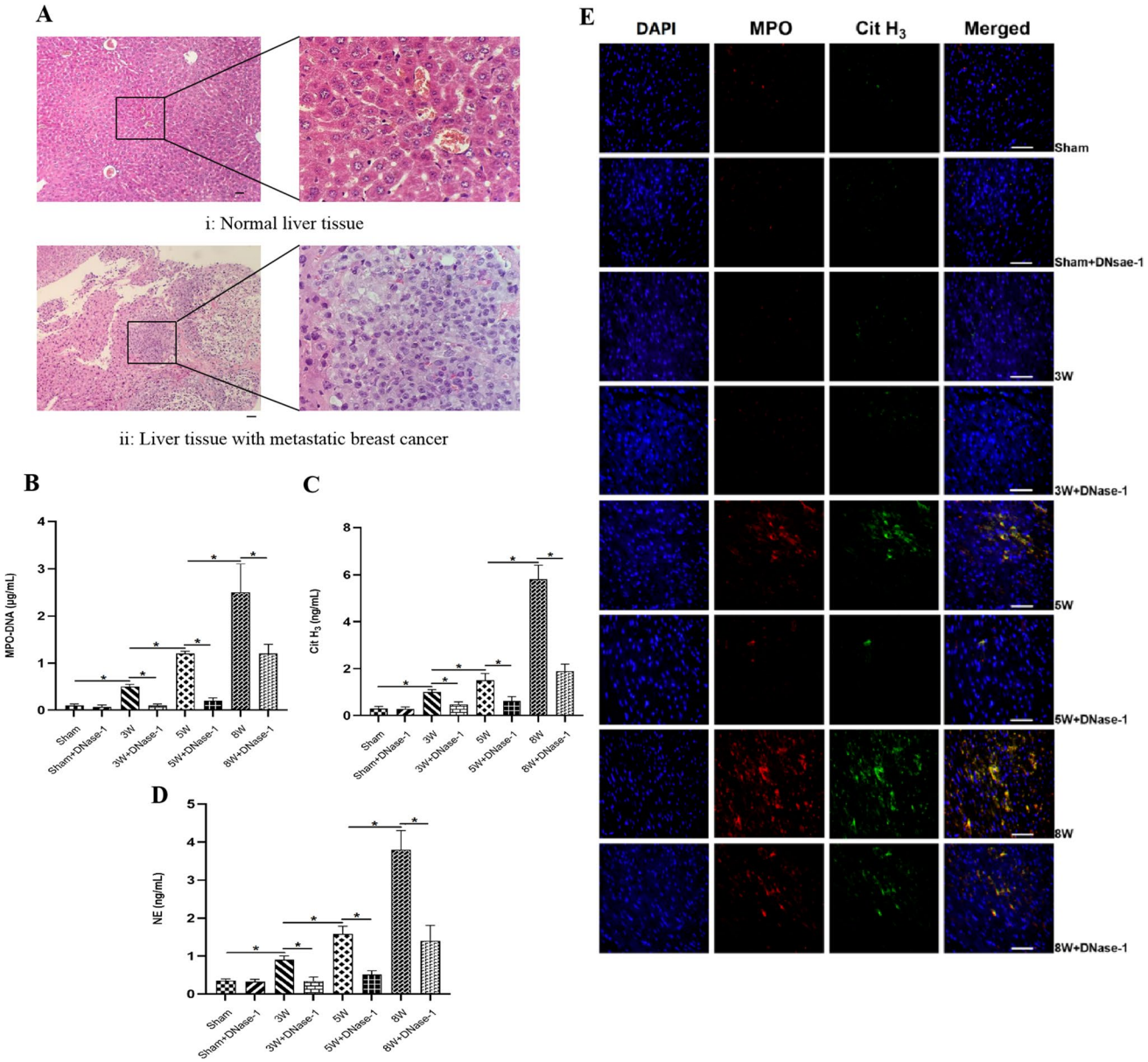

Fig. 1 Comparison of NETs in nude mouse of TNBC cells liver metastatic. The group of Sham + DNase-1, 3W + DNase-1, 5W + DNase-1, 8W + DNase-1 were intraperitoneal injected of DNase-1 (15 U/g) daily at the beginning, after injected MDA-MB-231 BC cells. **A** Normal liver tissue and liver tissue with metastatic BC by HE Staining (Scale bar, 50 μm). **B–D** The levels of NETs specific markers (MPO − DNA complex, Cit H_3, NE) in serum of nude mice by ELISA. **E** The distribution of NETs in nude mice cardiac tissue by Tissular Immunofluorescence Staining (Scale bar, 50 μm). $^{*}P < 0.05$. ($n = 5$)

and TNBC cells (MDA-MB-231). Among the cytokines tested, IL-8 exhibited the highest level (see Fig. 5A, B). Furthermore, in the serum of nude mice with TNBC liver metastasis, we observed a significant increase in IL-8 levels starting from the 3rd week after the injection of MDA-MB-231 cells. This elevated level was sustained at a consistently high value until the 8th week. However, the administration of DNase-1 did not impact the release of IL-8 (see Table 3; Fig. 5C).

CaSR through the NF-κB pathway regulated the secretion of IL-8 in TNBC

qRT-PCR, Western blot, as well as immunohistochemistry (IHC) techniques were utilized to examine TNBC tissues and cells. The findings demonstrated a notable increase in the levels of CaSR mRNA and protein (Fig. 6A–D). To explore the functional implications of this finding, we conducted experiments on MAD-MB-231 cells using specific

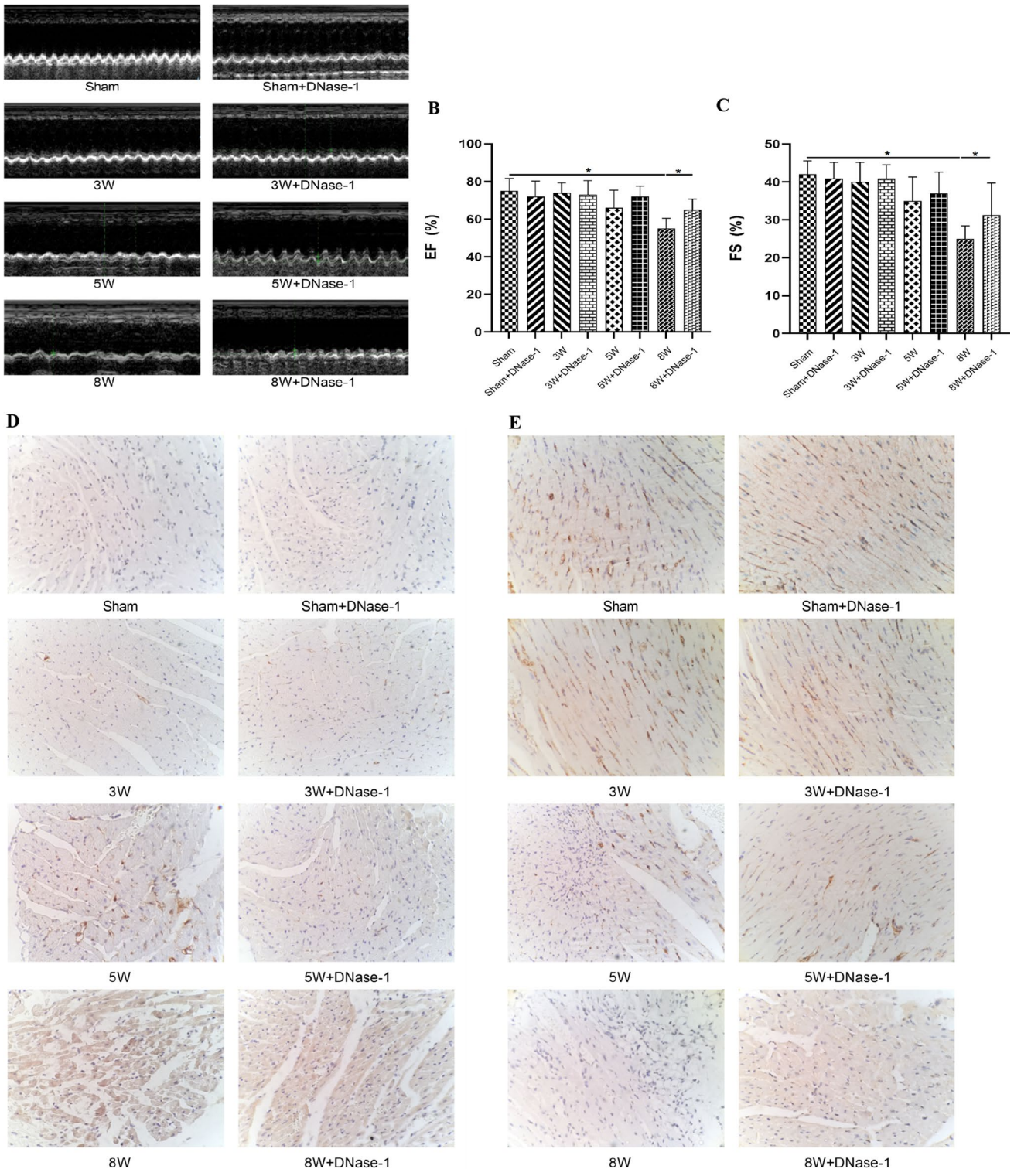

Fig. 2 Changes of heart in TNBC nude mice liver metastasis. **A–C** Ultrasound image of cardiac function by Echocardiography, statistical analysis of ejection fraction and Fractional shortening. **D, E** Bax and Bcl-2 expressions were determined through immunohistochemical staining (Scale bar, 50 μm). $^{*}P < 0.05$. ($n = 5$)

Table 1 Liver metastasis of different cardiac markers—changes in cardiac function in nude mice with TNBC metastatic

Group	Sham ($n=5$)	Sham + D ($n=5$)	3W ($n=5$)	3W + D ($n=5$)	5W ($n=5$)	5W + D ($n=5$)	8W ($n=5$)	8W + D ($n=5$)
E (cm/s)	68.09 ± 7.15	67.31 ± 7.97	66.96 ± 8.55	67.07 ± 7.61	68.11 ± 7.52	67.95 ± 8.14	70.64 ± 8.36	68.32 ± 10.07
A (cm/s)	45.05 ± 7.09	44.85 ± 6.97	43.98 ± 7.51	44.62 ± 6.85	43.67 ± 6.97	44.15 ± 6.69	38.14 ± 5.59	42.12 ± 6.31
E/A ratio	1.51 ± 0.08	1.50 ± 0.10	1.52 ± 0.06	1.50 ± 0.05	1.56 ± 0.16	1.53 ± 0.15	1.85 ± 0.61*	1.62 ± 0.23 ○
IVRT (m/s)	17.59 ± 2.04	17.32 ± 1.98	16.87 ± 2.54	17.51 ± 1.66	16.68 ± 2.17	17.44 ± 1.95	22.31 ± 3.94*	20.19 ± 1.22 ○
IVCT (m/s)	11.87 ± 1.74	12.41 ± 1.12	11.68 ± 1.69	11.97 ± 1.53	12.05 ± 1.34	11.84 ± 1.62	13.07 ± 2.17	11.87 ± 1.84
ET (m/s)	55.98 ± 5.61	56.02 ± 6.09	55.14 ± 5.89	55.47 ± 6.31	51.21 ± 5.29	54.98 ± 5.17	45.12 ± 6.12	50.51 ± 5.09
DT (m/s)	32.98 ± 5.43	33.17 ± 4.99	33.85 ± 4.68	33.51 ± 5.17	32.87 ± 5.62	31.85 ± 5.95	27.41 ± 7.34	30.67 ± 5.14
Tei index	0.54 ± 0.10	0.51 ± 0.12	0.50 ± 0.11	0.53 ± 0.06	0.56 ± 0.09	0.52 ± 0.11	0.71 ± 0.15*	0.63 ± 0.09○

*$P<0.05$ VS. Sham group, ○$P<0.05$ VS. 8W group

Table 2 Comparison of myocardial enzyme changes in nude mice of TNBC liver metastatic

Group	LDH (U/L)	MDA (mol/L)	SOD (U/mL)
Sham	184.21 ± 34.83	93.87 ± 25.65	148.79 ± 22.11
Sham + DNase-1	191.46 ± 29.01	98.46 ± 26.96	150.21 ± 25.36
3W	189.38 ± 34.97	96.41 ± 20.64	146.54 ± 29.48
3W + DNase-1	195.54 ± 31.95	94.52 ± 21.97	153.73 ± 20.87
5W	221.85 ± 35.36*	126.43 ± 26.81*	111.62 ± 19.45*
5W + DNase-1	194.46 ± 31.12◇	92.84 ± 28.73◇	130.48 ± 17.41◇
8W	294.76 ± 32.45△	176.56 ± 27.69△	84.67 ± 20.96△
8W + DNase-1	215.47 ± 46.24○	125.37 ± 24.18○	105.16 ± 19.53○

*$P<0.05$ VS. Sham group, ◇$P<0.05$ VS. 5W group, △$P<0.05$ VS. 5W group, ○$P<0.05$ VS. 8W group

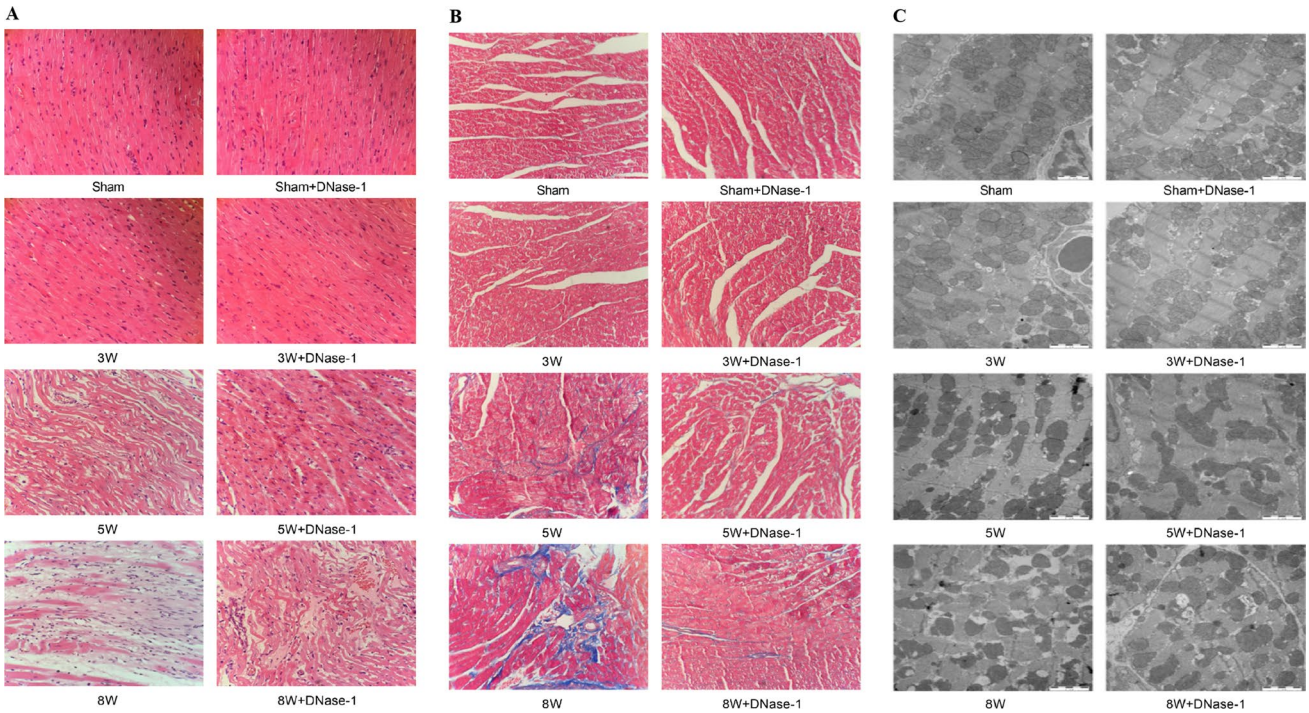

Fig. 3 Pathologic changes in cardiac tissue structure after liver metastasis in TNBC nude mice. **A** Structural changes of myocardial tissue by HE Staining (Scale bar, 50 μm). **B** Inflammatory changes of myocardial tissue by Masson Staining (Scale bar, 50 μm). **C** Myocardial tissue underwent ultrastructural changes observed through Transmission Electron Microscopy (Scale bar, 2 μm). *$P<0.05$. ($n=5$)

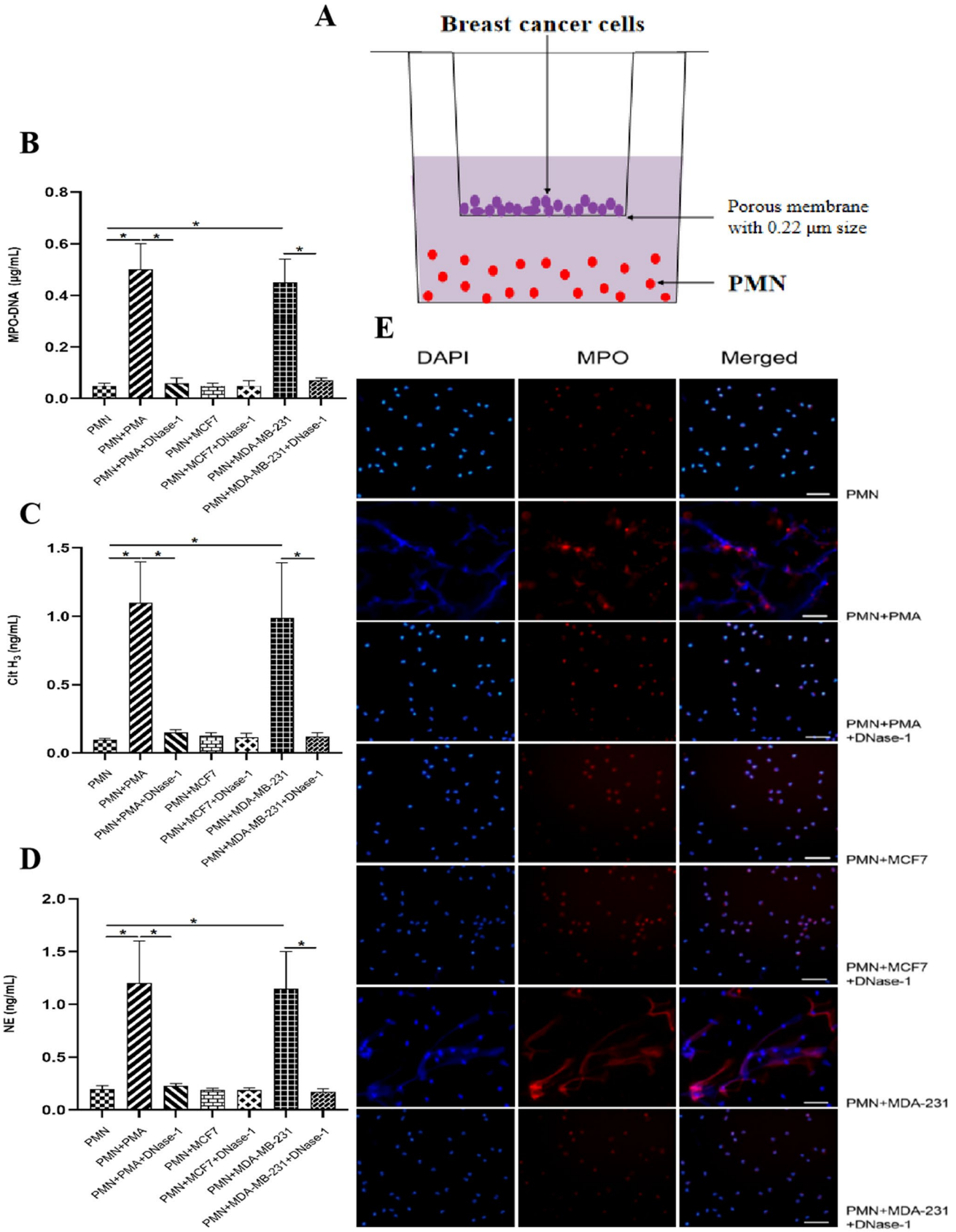
A
Breast cancer cells
Porous membrane
with 0.22 μm size
PMN
B
MPO-DNA (μg/mL)
0.8
0.6
0.4
0.2
0.0
PMN
PMN+PMA
PMN+PMA+DNase-1
PMN+MCF7
PMN+MCF7+DNase-1
PMN+MDA-MB-231
PMN+MDA-MB-231+DNase-1
C
Cit H3 (ng/mL)
1.5
1.0
0.5
0.0
D
NE (ng/mL)
2.0
1.5
1.0
0.5
0.0
E
DAPI
MPO
Merged
PMN
PMN+PMA
PMN+PMA +DNase-1
PMN+MCF7
PMN+MCF7 +DNase-1
PMN+MDA-231
PMN+MDA-231 +DNase-1

◂**Fig. 4** The identification of BC cells stimulated PMN to produce NETs. The group of PMA, MCF7, MDA-MB-231 were stimulated PMN with 25 nM PMA and nontriple-negative BC cells MCF7 or TNBC cells MAD-MB-231 for 4 h. The group of PMA + DNase-1, MCF7 + DNase-1, MDA-MB-231 + DNase-1 were PMN treated with 1 U/mL DNase-1 and incubated for 30 min, after the above stimulation. **A** The schema for PMN co-cultured with BC cells. **B–D** The levels of NETs specific markers (MPO − DNA complex, Cit H_3, NE) in cell culture supernatant by ELISA. The levels of NETs markers were significantly increased after PMA or MDA-MB-231 cells stimulated PMN, but DNase-1 could reverse these phenomena. **E** The identification of BC cells stimulates PMN to produce NETs by Cellular Immunofluorescence Staining. After PMA or MDA-MB-231 cells stimulated PMN, PMN formed a cloud of slender filamentous structures larger than itself, the phenomena of extracellular co-localization of MPO and DNA skeleton were obvious, but these cells structure could be inhibited by DNase-1 (Scale bar, 20 μm). $^{*}P < 0.05$. ($n = 5$)

Table 3 Comparison of IL-8 level in nude mice of TNBC liver metastatic

Group	IL-8 (pg/ml)
Sham	67.14 ± 18.27
Sham + DNase-1	58.62 ± 20.29
3W	1975.53 ± 315.68*
3W + DNase-1	2019.34 ± 309.45
5W	2057.29 ± 359.74
5W + DNase-1	1998.86 ± 378.65
8W	2095.31 ± 345.23
8W + DNase-1	2037.24 ± 349.81

*$P < 0.05$ VS. Sham group

compounds: a CaSR agonist, Cinacalcet (CIN), a CaSR inhibitor named NPS 2134 (NPS), and a NF-κB pathway inhibitor referred to as PDTC. Our findings revealed that the CaSR agonist had a notable impact on the NF-κB pathway protein p65, including enhanced phosphorylation. In addition, it upregulated the expression of IL-8 mRNA and protein, while also stimulating the secretion of IL-8. Conversely, the administration of the CaSR inhibitor, NF-κB pathway inhibitor, or a combination of both successfully reversed these observed changes (Fig. 6E–H; Table 4).

The activity of MDA-MB-231 cells in inducing the formation of NETs by PMN was controlled by CaSR

To investigate the involvement of CaSR in MDA-MB-231 cell-induced formation of NETs by polymorphonuclear leukocytes (PMN), PMN cells were co-cultured with MDA-MB-231 cells under different conditions for a duration of 4 h. Our findings suggested that the activation of CaSR in MDA-MB-231 cells significantly potentiated the stimulation of PMN, leading to an increased formation of NETs as compared to the group with MDA-MB-231 cells alone. This effect was evidenced through increased expression of markers associated with NETs and enhanced co-localization of MPO and extracellular DNA when compared with the MDA-MB-231 group. When the activation of CaSR was suppressed or the NF-κB pathway was obstructed, MDA-MB-231 cells demonstrated an impaired capability to induce the generation of PMN-driven NETs (Fig. 7A–D).

Effects of CaSR-regulated MDA-MB-231on cardiomyocytes injury through PMN-generated NETs

To investigate the effects on neonatal mouse cardiomyocytes, co-culture experiments were performed by combining polymorphonuclear leukocytes (PMN) with supernatants derived from MDA-MB-231 cells, which had been treated with a CaSR agonist, CaSR inhibitor, and an inhibitor of the NF-κB pathway. The collected supernatants were then utilized to co-culture neonatal mouse cardiomyocytes for a

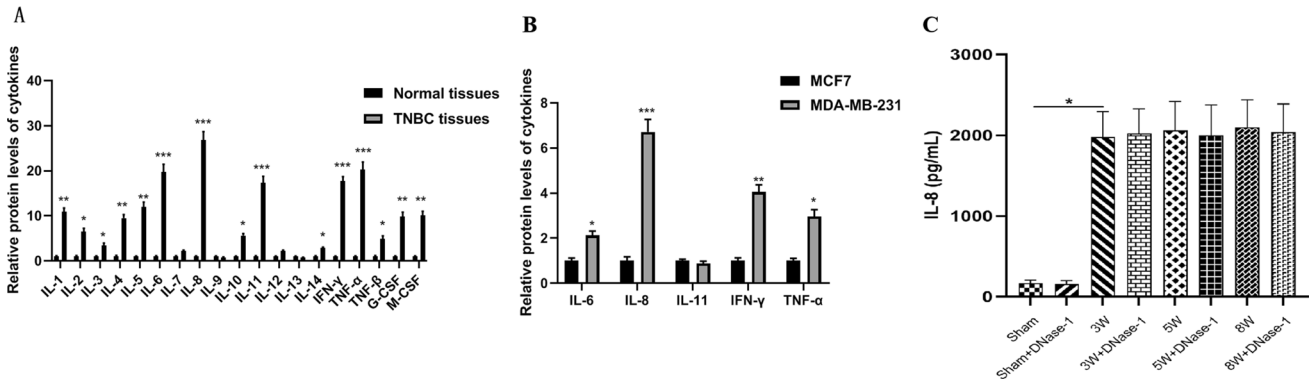

Fig. 5 The levels of cytokines in BC. **A** Statistical analysis of cytokines levels between BC patients and normal group. **B** Statistical analysis of cytokines levels secreted by BC cells. **C** Statistical analysis of IL-8 level in nude mice of TNBC MDA-MB-231 cells liver metastasis. *$P < 0.05$, ***$P < 0.001$. ($n = 5$)

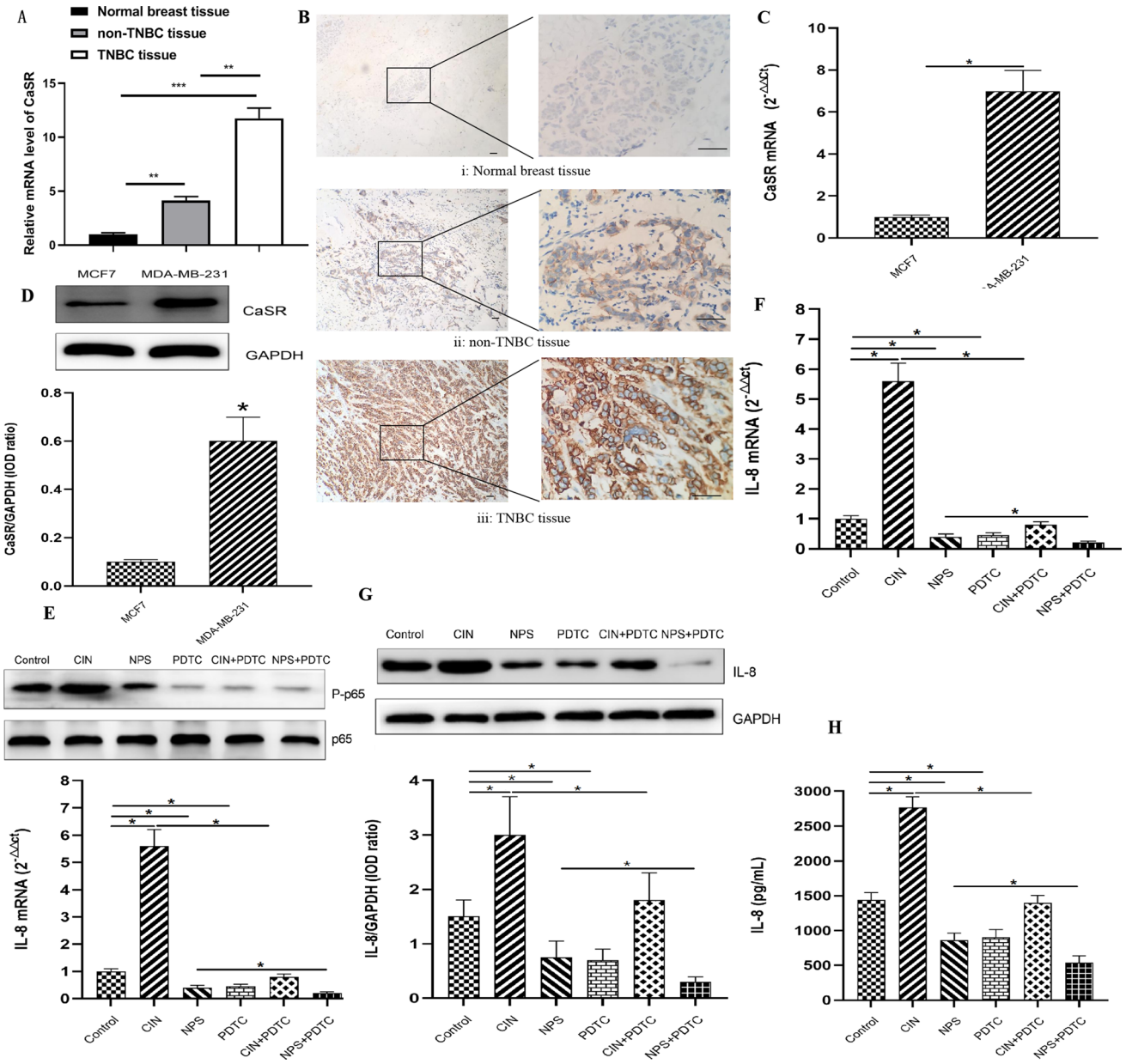

Fig. 6 The regulation of IL-8 secretion in TNBC through the NF-κB pathway by CaSR. **A–B** The statistical analysis of CaSR mRNA expression in breast tissue and BC tissue is presented along with the immunohistochemical staining of CaSR protein (scale bar, 50 μm). **C–D** The statistical analysis of CaSR mRNA expression in BC cells, the measurement of CaSR protein expression through Western Blot, and the statistical analysis of CaSR protein results. In panels (E–H), MDA-MB-231 cells were subjected to different treatments (Cinacalcet, NPS 2143, PDTC, Cinacalcet + PDTC, and NPS 2143 + PDTC) for 30 min. **E** The measurement and statistical analysis of P-p65 protein expression through Western Blot. **F** The statistical analysis of IL-8 mRNA expression. **G** The measurement and statistical analysis of IL-8 protein expression through Western Blot. **H** The statistical analysis of IL-8 secretion. $*P < 0.05$. CIN: Cinacalcet, NPS: NPS 2143. ($n = 5$)

duration of 24 h. Various parameters, such as cardiomyocyte apoptosis rate, ultrastructure, and myocardial enzyme levels, were assessed using flow cytometry, transmission electron microscopy (TEM), and ELISA, respectively. Our findings demonstrated that the CIN + PMN + MDA-MB-231 group exhibited significantly higher cardiomyocyte apoptosis rate, greater ultrastructural damage, and altered myocardial enzyme levels, accompanied by elevated levels of NETs, compared to the PMN + MDA-MB-231 group. In contrast, the other groups, where NETs formation was absent, showed significantly reduced cardiomyocyte damage (Fig. 8A–C; Table 5 and 6).

Table 4 Comparison of IL-8 level in different groups

Group	IL-8 (pg/ml)
MDA-MB-231	1438.76 ± 102.78
MDA-MB-231 + CIN	2765.91 ± 153.63*
MDA-MB-231 + NPS	864.25 ± 97.51△
MDA-MB-231 + PDTC	903.76 ± 110.48◇
MDA-MB-231 + CIN + PDTC	1397.36 ± 105.23○
MDA-MB-231 + NPS + PDTC	537.28 ± 96.97☆

*$P < 0.05$ VS. MDA-MB-231 group, △$P < 0.05$ VS. MDA-MB-231 group, ◇$P < 0.05$ VS.MDA-MB-231gruop, ○$P < 0.05$ VS. MDA-MB-231 + CIN group, ☆$p < 0.05$ VS. MDA-MB-231 + NPS group

Discussion

BC patients have a significantly increased absolute risk (ranging between 1.6% and 10.4%) of CVD-related mortality compared to women without BC [41]. The intersection of BC and CVD biology has become a trending topic. Currently, clinical symptoms, electrocardiogram, and myocardial enzymes serve as the primary basis for CVD clinical diagnosis [42]. However, it is essential to develop personalized and evidence-based strategies to enhance the quality of life for BC patients who also suffer from CVD. In our study, we observed that BC patients with CVD were older with higher clinical stage, higher pathological grade, and higher levels of NETs markers compared to BC patients without CVD. Specifically, individuals with TNBC are at a higher risk of CVD. These results indicate that NETs may have the potential to function as predictive markers for assessing CVD risk in BC patients.

Juwon Park et al. previously reported a correlation between the presence of NETs and the metastatic burden in TNBC. They discovered that both 4T1 cells as well as C3(1)-Tag tumors, which serve as models of TNBC, have the ability to induce polymorphonuclear (PMN) cells to enhance NETs formation. Furthermore, they observed higher levels of NETs production in TNBC clinical samples compared to other subtypes [43]. Linbin Yang et al. also found that MDA-MB-231 cells, aTNBC model, produced more NETs during liver metastasis [40]. To investigate the essential role of NETs in BC with CVD, we constructed a TNBC liver metastatic nude mice model. In these mice models, we observed a gradual increase in NETs markers (MPO-DNA complex, Cit H_3, NE) levels in the peripheral blood, as well as the deposition of NETs around cardiac tissue, as the injection time of MDA-MB-231 cells extended. Concurrently, we observed a gradual impairment in the heart function of the nude mice. However, when we injected DNase-1, which can digest NETs, we observed a reversal of the aforementioned changes, leading to improved cardiac function. These results suggest that excessive production and accumulation of NETs in BC can impair cardiac function, and inhibiting NETs production may have practical application value in treating and preventing BC with CVD.

The involvement of cytokines in NET formation is particularly notable in the context of inflammatory diseases. An et al. observed elevated levels of the pro-inflammatory cytokine IL-8 and a higher presence of NETs in the serum of patients with atherosclerosis (AS). They demonstrated that the interaction between IL-8 and its receptor CXCR2 on PMN triggered the formation of NETs, thereby exacerbating AS progression in vivo. This process was mediated by the signaling pathways of Src, ERK MAPK, and p38 MAPK [44]. Similarly, a positive feedback loop was identified by Yang et al., wherein elevated tumor levels of IL-8 and NETs mutually reinforced each other, promoting the metastasis of colorectal cancer to the liver [45].

In our study, we observed that TNBC MDA-MB-231 cells, but not non-TNBC MCF7 cells, had the capability to stimulate PMN to produce NETs. This effect was attributed to the higher levels of IL-8 found in the supernatants of MDA-MB-231 cells compared to MCF7 cells. In addition, elevated IL-8 levels were detected in the serum of BC patients with CVD and in liver metastasis mouse models. Therefore, we consider IL-8 to be a key factor in the development of CVD in BC patients, as it influences PMN to initiate NETs formation.

Earlier investigations have shown that the CaSR is expressed in T lymphocytes found in human peripheral blood. Upon activation, CaSR triggers the release of IL-6 and TNF-β through the involvement of the NF-κB and MAPKs signaling pathways in the context of Acute Myocardial Infarction (AMI) [32, 35]. Zhai et al. identified that the activated CaSR in PMN enhances the release of IL-6 and MPO through the NF-κB signaling pathway, supporting these findings [33]. The study of Gao Q et al. indicated that the NF-κB signaling pathway can up-regulate the expression of IL-8 [46]. Based on these outcomes, we investigated the relationship between CaSR and cytokines in our study. Our findings verified a significant upregulation of CaSR expression in both TNBC tissues and TNBC -derived MDA-MD-231 cells. In addition, activation of CaSR in MDA-MD-231 cells resulted in heightened secretion of IL-8 and increased expression of P-p65, a protein associated with the NF-kB pathway. We observed that inhibiting CaSR and/or blocking the NF-κB pathway reversed these changes and suppressed PMN from forming NETs. Although there was no clear evidence that the specific CaSR-NF-κb-iL-8 axis directly caused myocardial damage in patients, our study fills this gap.

In light of our findings and extant research, it becomes evident that a more comprehensive exploration of environmental factors would enhance our understanding of the intricate mechanisms involved in the interplay between BC

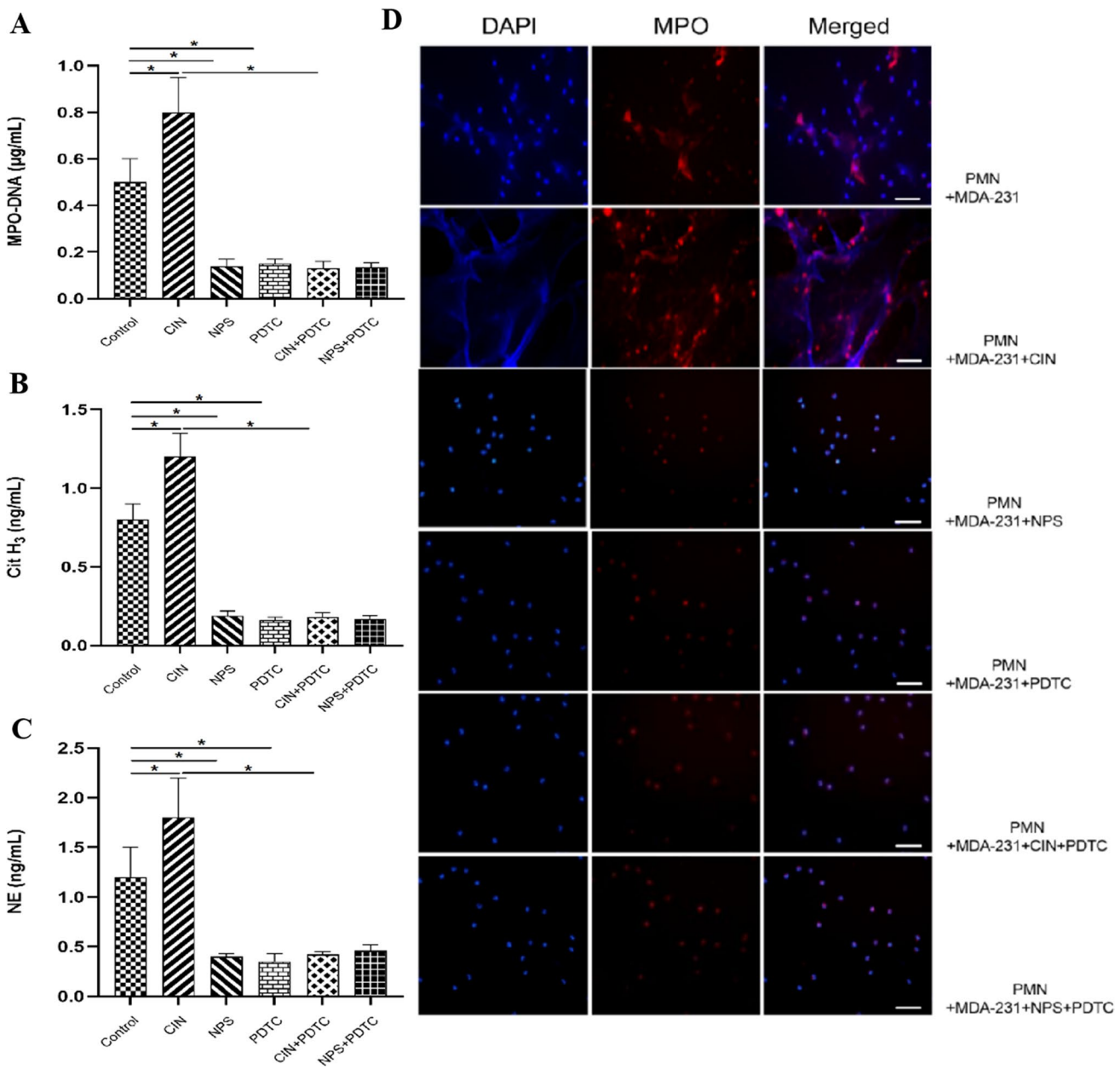

Fig. 7 CaSR regulates the effect of MDA-MB-231 on the formation of NETs in PMN. After a 30-min incubation with various compounds (Cinacalcet, NPS 2143, PDTC, Cinacalcet + PDTC, NPS 2143 + PDTC) at a concentration of 100 nM, MDA-MB-231 cells were co-cultured with PMN for a duration of 4 h. **A–C** ELISA was performed to measure the levels of specific NETs markers (MPO-DNA complex, Cit H_3, NE) in the cell culture supernatant. **D** The stimulation of PMN to produce NETs in response to BC cells was confirmed through Cellular Immunofluorescence Staining, with a scale bar of 20 μm. Statistical analysis indicated significance at $^*P < 0.05$. ($n = 5$)

and CVD. The environment, both internal (physiological or biochemical) and external (physical or cultural), has been consistently signaled as a potential contributor to cancer and CVD pathogenesis. The detailed processes or pathways through which these environmental factors exert their influence on disease development, however, are still the subject of ongoing research. One critical connection and starting point of these may lies in the environmental modulation of the CaSR.

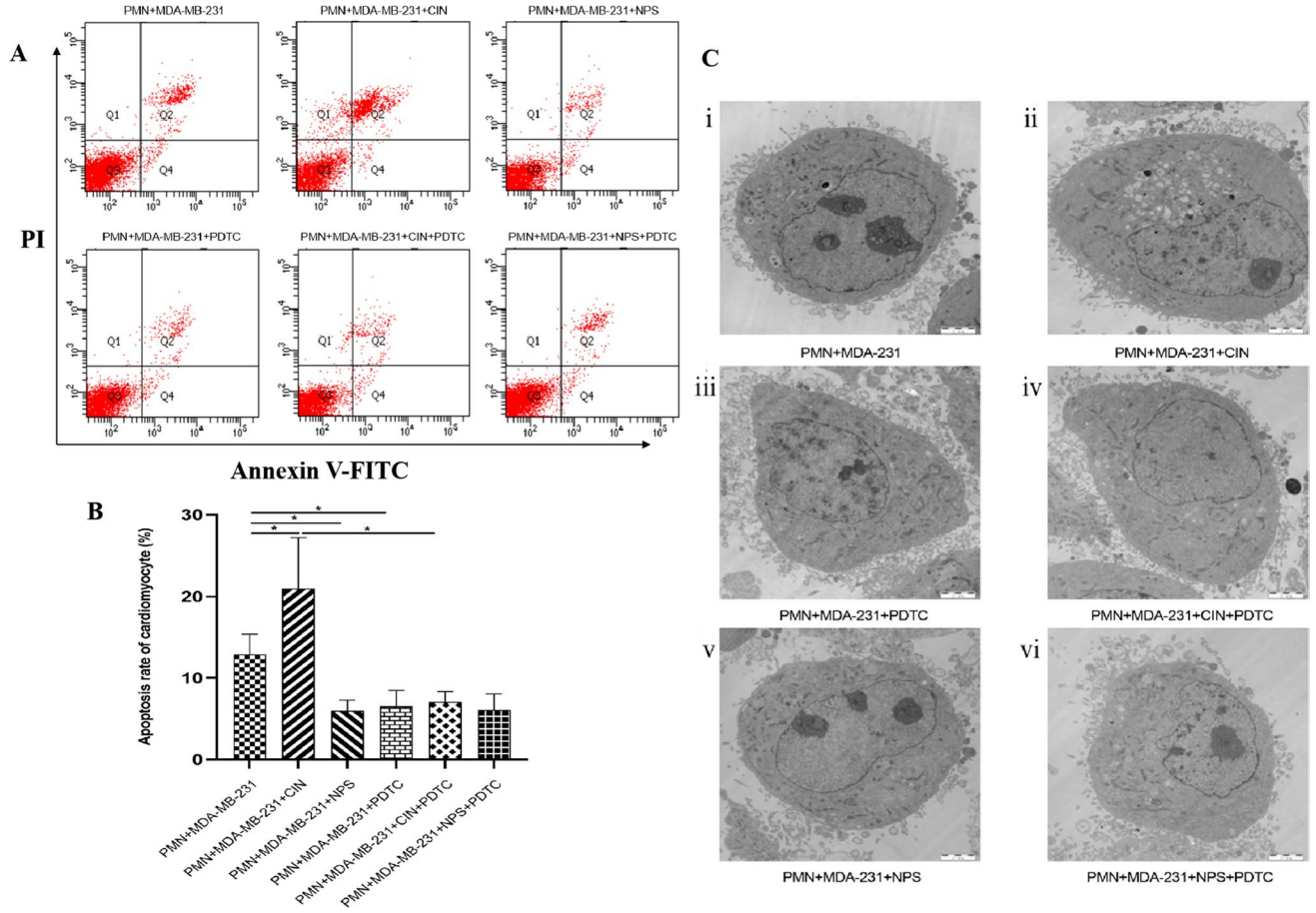

Fig. 8 Effects of CaSR-regulated MDA-MB-231 stimulated PMN-generated NETs on cardiomyocytes **A**, **B** The results of myocardial apoptosis were detected by Flow Cytometry; Results of Statistical Analysis. **C** Ultrastructural changes of Cardiomyocyte (Scale bar, 2 μm). i In the supernatants of MDA-MB-231 and PMN co-cultured, the myocardial cells membrane was intact, the nucleus were slightly shrunk, the shape was irregular, the chromatin was slightly condensed, the number of mitochondria in the cytoplasm was increased, the mitochondrial membrane was intact, the swelling was slight, the internal crest structure was slightly disordered, and a few vacuoles were formed. The myofilaments were slightly disorganized in the cytoplasm, and only a few of the endoplasmic reticulum were slightly dilated. ii In the supernatants of CaSR activated MDA-MB-231 and PMN co-cultured, the degree of myocardial cells damage was more obvious. iii–vi The morphology of cardiomyocytes was basically normal. $^{*}P<0.05$. ($n=5$)

Table 5 The effects of NETs on myocardial apoptosis rate

Group	Myocardial apoptosis rate (%)
PMN + MDA-MB-231	12.89 ± 2.49
PMN + MDA-MB-231 + CIN	20.97 ± 6.22*
PMN + MDA-MB-231 + NPS	5.98 ± 1.31$^{\triangle}$
PMN + MDA-MB-231 + PDTC	6.55 ± 1.93$^{\diamond}$
PMN + MDA-MB-231 + CIN + PDTC	7.06 ± 1.27$^{\bigcirc}$
PMN + MDA-MB-231 + NPS + PDTC	6.06 ± 1.99

$^{*}P<0.05$ VS. MDA-MB-231 group, $^{\triangle}P<0.05$ VS. MDA-MB-231 group, $^{\diamond}P<0.05$ VS. MDA-MB-231 group, $^{\bigcirc}P<0.05$ VS. MDA-MB-231 + CIN group

Table 6 The effects of NETs on myocardial enzyme secretion

Group	LDH (U/L)	MDA (mol/L)	SOD (U/mL)
PMN + MDA-MB-231	177.68 ± 32.85	44.83 ± 16.46	39.27 ± 8.75
PMN + MDA-MB-231 + CIN	238.54 ± 44.19*	67.41 ± 19.92*	21.98 ± 10.64*
PMN + MDA-MB-231 + NPS	79.35 ± 15.76$^{\triangle}$	11.85 ± 3.28$^{\triangle}$	55.43 ± 9.85$^{\triangle}$
PMN + MDA-MB-231 + PDTC	76.87 ± 12.39$^{\diamond}$	10.97 ± 4.13$^{\diamond}$	54.54 ± 11.37$^{\diamond}$
PMN + MDA-MB-231 + CIN + PDTC	80.64 ± 19.31°	9.89 ± 5.67°	56.28 ± 13.79°
PMN + MDA-MB-231 + NPS + PDTC	77.26 ± 16.79	11.27 ± 3.64	51.98 ± 9.66

*$P < 0.05$ VS. MDA-MB-231 group, $^{\triangle}P < 0.05$ VS. MDA-MB-231 group, $^{\diamond}P < 0.05$ VS. MDA-MB-231 group, $^{\circ}P < 0.05$ VS. MDA-MB-231 + CIN group

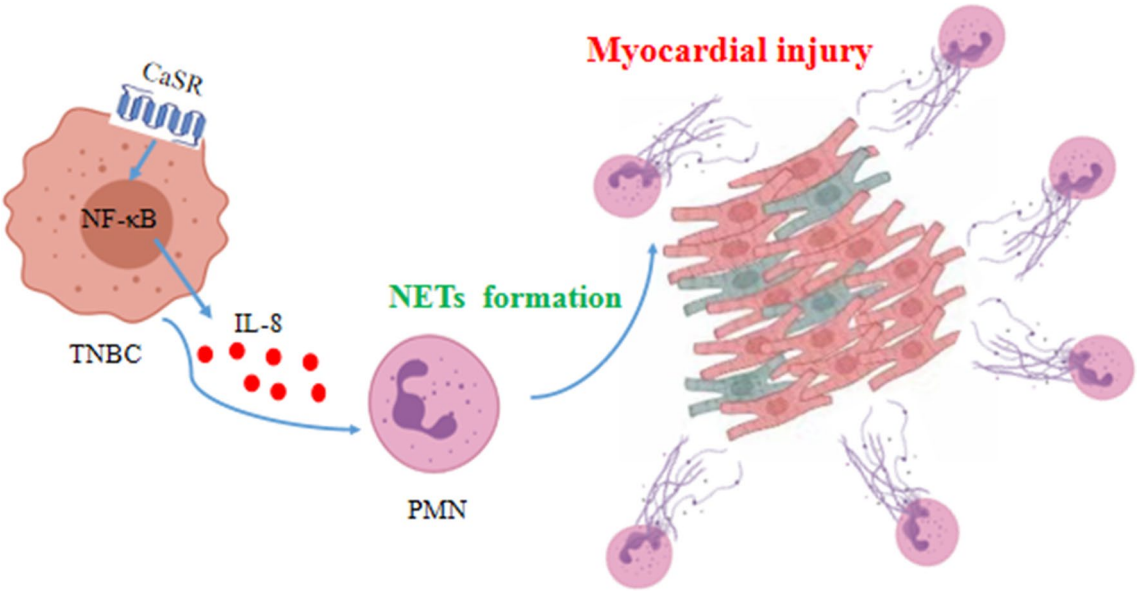

Fig. 9 The diagrammatic representation showcasing the impact of CaSR on the promotion of NETs formation and the induction of myocardial injury in TNBC. By modulating the secretion of the cytokine IL-8 in MDA-MB-231 cells and influencing the ability of PMN to form NETs, CaSR plays a role in causing myocardial injury that might be associated with the NF-κB signaling pathway

Environmental factors such as diet, specifically the intake of calcium, have shown impacts on CaSR expression levels. Surges in dietary calcium act as an activator for CaSR, which we established to hold a pivotal role in promoting the pro-inflammatory states conducive to both BC progression (particularly in TNBC) and CVD [36].

Furthermore, studies have shown that increased levels of environmental pollutants capable of acting as endocrine disruptors can lead to both TNBC progression and CVD by dysregulating calcium homeostasis [47]. These disruptors might hyperactivate CaSR, leading to the overproduction of proinflammatory cytokines such as IL-8, and thus the induction of NETs formation which exacerbates both conditions [48].

Neoplasms remain the main killer worldwide [49–58]. The typical Western diet, typified by high consumption of processed foods and red meat, has been associated with a rise in systemic inflammation [56, 59]. The activation of inflammatory pathways, including the NF-κB pathway, directly links to the progression of both TNBC and CVD. This dietary pattern may indirectly affect CaSR function and further contribute to the inflammatory status.

This study has several important clinical implications. First, it identifies circulating NETs as a potential biomarker to stratify BC patients at high risk of developing CVD, which could guide targeted preventive strategies in susceptible individuals. Validation of NETs as a predictive biomarker could be rapidly translated to the clinic using existing assays. Second, it proposes NETs as a modifiable therapeutic target to mitigate CVD risk in BC patients. Strategies to inhibit NETs formation or enhance their degradation, such as DNase treatment, could be tested for cardioprotective effects in prospective clinical trials. Third, it highlights the calcium-sensing receptor (CaSR) as a regulator of NETs production in triple

negative breast cancer. CaSR may represent a novel drug target to dampen systemic inflammation and prevent cardiac complications. CaSR inhibitors could be repurposed or developed for testing in BC patients. Fourth, these findings reveal an under-recognized connection between BC, inflammation, and CVD that warrants closer surveillance of cardiac health in BC survivors, especially those with triple negative disease. Patients could be screened for circulating NETs levels and early signs of CVD to enable timely interventions. Finally, this study underscores the need to determine the cardiotoxic effects of various BC therapies, as some may inadvertently promote NETs formation and increase CVD risk. Incorporating cardiac monitoring in BC clinical trials is imperative.

This study has several limitations that should be acknowledged. First, the sample size of BC patients and controls was relatively small, which limits the statistical power and generalizability of the findings. A larger cohort is needed to validate the association between NETs levels and CVD risk in BC patients. Second, this was a cross-sectional study measuring NETs at a single timepoint, which precludes determining causality between NETs and CVD development. Longitudinal studies tracking NETs levels over time are required to establish temporal relationships. Third, we evaluated NETs systemic levels but did not assess local cardiac levels, which could more directly demonstrate the involvement of NETs in myocardial damage. Fourth, the use of cell lines and animal models may not fully recapitulate the complex biology of human cancers and CVD. Further studies in humans are warranted to translate these findings to the clinic. Finally, we did not explore the impact of cancer treatments on NETs production and the development of CVD. Evaluating how different therapeutic regimens influence NETs levels and CVD risk has important clinical implications. Overall, this study provides preliminary evidence linking NETs to CVD in BC patients, but further research is needed to validate these findings and uncover the underlying mechanisms.

In conclusion, this study found that CaSR could affect IL-8 production from TNBC cells through the NF-kB signaling pathway, influencing the ability of PMN to form NETs and subsequently damaging cardiomyocytes (Fig. 9). In the future study, it is crucial to underscore the importance of exploring the potential preventative measures, which might include modifications to diet or reductions in exposure to certain environmental pollutants, with the aims to modulate CaSR function, and ultimately decrease the incidence of CVD in BC patients.

Conclusions

The study sheds light on the potential impact of NETs in understanding the increased vulnerability of BC patients to CVD. A positive association was found between NETs concentration in the peripheral blood and the elevated risk of CVD in BC patients. This establishes NETs as a promising biological biomarker and a novel target for preventive interventions against CVD in individuals affected by BC.

Acknowledgements Not applicable.

Author contributions JZ and YC contributed equally to this study. All authors contributed to the study conception and design. Material preparation, data collection and analysis were performed by WX, XL and CD. The first draft of the manuscript was written by YS and all authors commented on previous versions of the manuscript. All authors read and approved the final manuscript.

Funding This study has received support from the Natural Science Foundation of Heilongjiang Province, China (LH2021H082).

Data availability The article incorporates the pertinent data utilized to substantiate the findings of this study.

Declarations

Conflict of interest The authors have declared that no conflict of interest exists.

Ethical approval Animal experiments were approved and supervised by the Animal Ethics Committee of Harbin Medical University. All methods were carried out in accordance with relevant guidelines and regulations.

Consent to publish Not applicable.

References

1. Cree IA, Ruiz BII, Zavadil J, McKay J, Olivier M, Kozlakidis Z et al (2021) The international collaboration for cancer classification and research. Int J Cancer 148:560–571
2. Chlebowski RT, Anderson GL, Aragaki AK, Manson JE, Stefanick ML, Pan K et al (2020) Association of menopausal hormone therapy with breast cancer incidence and mortality during long-term follow-up of the women's health initiative randomized clinical trials. JAMA 324:369–380
3. Henry ML, Niu J, Zhang N, Giordano SH, Chavez-MacGregor M (2018) Cardiotoxicity and cardiac monitoring among chemotherapy-treated breast cancer patients. JACC Cardiovasc Imaging 11:1084–1093
4. Abe J-I, Yusuf SW, Deswal A, Herrmann J (2020) Cardio-oncology: learning from the old, applying to the new. Front Cardiovasc Med 7:601893
5. Barish R, Lynce F, Unger K, Barac A (2019) Management of cardiovascular disease in women with breast cancer. Circulation 139:1110–1120
6. Archer M, Dogra N, Kyprianou N (2020) Inflammation as a driver of prostate cancer metastasis and therapeutic resistance. Cancers (Basel) 12:2984
7. Zittan E, Gralnek IM, Berns MS (2020) The new proactive approach and precision medicine in Crohn's disease. Biomedicines 8:193
8. Gough P, Myles IA (2020) Tumor necrosis factor receptors: pleiotropic signaling complexes and their differential effects. Front Immunol 11:585880

9. Aisiku IP, Yamal J-M, Doshi P, Benoit JS, Gopinath S, Goodman JC et al (2016) Plasma cytokines IL-6, IL-8, and IL-10 are associated with the development of acute respiratory distress syndrome in patients with severe traumatic brain injury. Crit Care 20:288
10. Vachharajani V, McCall CE (2020) Sirtuins: potential therapeutic targets for regulating acute inflammatory response? Expert Opin Ther Targets 24:489–497
11. van der Meijden PEJ, Heemskerk JWM (2019) Platelet biology and functions: new concepts and clinical perspectives. Nat Rev Cardiol 16:166–179
12. Wilde B, Katsounas A (2019) Immune dysfunction and albumin-related immunity in liver cirrhosis. Mediators Inflamm 2019:7537649
13. Smids C, Horjus CS, Horje T, Drylewicz J, Roosenboom B, Groenen MJM, van Koolwijk E et al (2018) Intestinal T cell profiling in inflammatory bowel disease: linking t cell subsets to disease activity and disease course. J Crohns Colitis 12:465–475
14. Ershaid N, Sharon Y, Doron H, Raz Y, Shani O, Cohen N et al (2019) NLRP3 inflammasome in fibroblasts links tissue damage with inflammation in breast cancer progression and metastasis. Nat Commun 10:4375
15. Hajizadeh F, Maleki LA, Alexander M, Mikhailova MV, Masjedi A, Ahmadpour M et al (2021) Tumor-associated neutrophils as new players in immunosuppressive process of the tumor microenvironment in breast cancer. Life Sci 264:118699
16. Döring Y, Libby P, Soehnlein O (2020) Neutrophil extracellular traps participate in cardiovascular diseases: recent experimental and clinical insights. Circ Res 126:1228–1241
17. Moschonas IC, Tselepis AD (2019) The pathway of neutrophil extracellular traps towards atherosclerosis and thrombosis. Atherosclerosis 288:9–16
18. de Bont CM, Boelens WC, Pruijn GJM (2019) NETosis, complement, and coagulation: a triangular relationship. Cell Mol Immunol 16:19–27
19. Kang L, Huilin Yu, Yang X, Zhu Y, Bai X, Wang R et al (2020) Neutrophil extracellular traps released by neutrophils impair revascularization and vascular remodeling after stroke. Nat Commun 11:2488
20. Snoderly HT, Boone BA, Bennewitz MF (2019) Neutrophil extracellular traps in breast cancer and beyond: current perspectives on NET stimuli, thrombosis and metastasis, and clinical utility for diagnosis and treatment. Breast Cancer Res 21:145
21. Mutua V, Gershwin LJ (2021) A review of neutrophil extracellular traps (NETs) in disease: potential anti-NETs therapeutics. Clin Rev Allergy Immunol 61:194–211
22. Demers M, Krause DS, Schatzberg D, Martinod K, Voorhees JR, Fuchs TA et al (2012) Cancers predispose neutrophils to release extracellular DNA traps that contribute to cancer-associated thrombosis. Proc Natl Acad Sci USA 109:13076–81
23. Xiao Y, Cong M, Li J, He D, Qiuyao Wu, Tian Pu et al (2021) Cathepsin C promotes breast cancer lung metastasis by modulating neutrophil infiltration and neutrophil extracellular trap formation. Cancer Cell 39:423–437
24. Jiménez-Alcázar M, Rangaswamy C, Panda R, Bitterling J, Simsek YJ, Long AT et al (2017) Host DNases prevent vascular occlusion by neutrophil extracellular traps". Science 358:1202–1206
25. Pertiwi KR, van der Wal AC, Pabittei DR, Mackaaij C, van Leeuwen MB, Li X et al (2018) Neutrophil extracellular traps participate in all different types of thrombotic and haemorrhagic complications of coronary atherosclerosis. Thromb Haemost 118:1078–1087
26. Leach K, Hannan FM, Josephs TM, Keller AN, Møller TC, Ward DT et al (2020) International union of basic and clinical pharmacology. CVIII. Calcium-sensing receptor nomenclature, pharmacology, and function. Pharmacol Rev 72:558–604
27. Tuffour A, Kosiba AA, Zhang Y, Peprah FA, Jie G, Shi H (2021) Role of the calcium-sensing receptor (CaSR) in cancer metastasis to bone: identifying a potential therapeutic target. Biochim Biophys Acta Rev Cancer 1875:188528
28. Yang W, Liu L, Masugi Y, Qian ZR, Nishihara R, Keum NN et al (2018) Calcium intake and risk of colorectal cancer according to expression status of calcium-sensing receptor (CASR). Gut 67:1475–1483
29. Das S, Clézardin P, Kamel S, Brazier M, Mentaverri R (2020) The CaSR in pathogenesis of breast cancer: a new target for early stage bone metastases. Front Oncol 10:69
30. Hannan FM, Kallay E, Chang W, Brandi ML, Thakker RV (2018) The calcium-sensing receptor in physiology and in calcitropic and noncalcitropic diseases. Nat Rev Endocrinol 15:33–51
31. Li T, Sun M, Yin X, Chunli Wu, Qiuyue Wu, Feng S et al (2013) Expression of the calcium sensing receptor in human peripheral blood T lymphocyte and its contribution to cytokine secretion through MAPKs or NF-κB pathways. Mol Immunol 53:414–420
32. Zeng J-Y, Jing-Jing Du, Pan Y, Jian Wu, Bi H-L, Cui B-H et al (2016) Calcium-sensing receptor in human peripheral blood t lymphocytes is involved in the AMI onset and progression through the NF-κB signaling pathway. Int J Mol Sci 17:1397
33. Zhai T-Y, Cui B-H, Zou L, Zeng J-Y, Gao S, Zhao Q et al (2017) Expression and role of the calcium-sensing receptor in rat peripheral blood polymorphonuclear neutrophils. Oxid Med Cell Longev 2017:3869561
34. Zhu D, Zhang Y, Wang S (2021) Histone citrullination: a new target for tumors. Mol Cancer 20:90
35. Zeng J, Pan Y, Cui B, Zhai T, Gao S, Zhao Q et al (2018) Calcium-sensing receptors in human peripheral T lymphocytes and AMI: cause and effect. Int J Mol Med 42:3437–3446
36. Albrengues J, Shields MA, David NG, Park CG, Ambrico A, Poindexter ME et al (2018) Neutrophil extracellular traps produced during inflammation awaken dormant cancer cells in mice. Science 361:4227
37. Lachowicz-Scroggins ME, Dunican EM, Charbit AR, Raymond W, Looney MR, Peters MC et al (2019) Extracellular DNA, neutrophil extracellular traps, and inflammasome activation in severe asthma. Am J Respir Crit Care Med 199:1076–1085
38. Yagi Y, Aly RG, Tabata K, Barlas A, Rekhtman N, Eguchi T et al (2020) Three-dimensional histologic, immunohistochemical, and multiplex immunofluorescence analyses of dynamic vessel Co-option of spread through air spaces in lung adenocarcinoma. J Thorac Oncol 15:589–600
39. Frangou E, Chrysanthopoulou A, Mitsios A, Kambas K, Arelaki S, Angelidou I et al (2019) REDD1/autophagy pathway promotes thromboinflammation and fibrosis in human systemic lupus erythematosus (SLE) through NETs decorated with tissue factor (TF) and interleukin-17A (IL-17A). Ann Rheum Dis 78:238–248
40. Yang L, Liu Q, Zhang X, Liu X, Zhou B, Chen J et al (2020) DNA of neutrophil extracellular traps promotes cancer metastasis via CCDC25. Nature 583:133–138
41. Kirkham AA, Beaudry RI, Ian Paterson D, Mackey JR, Haykowsky MJ (2019) Curing breast cancer and killing the heart: a novel model to explain elevated cardiovascular disease and mortality risk among women with early stage breast cancer. Prog Cardiovasc Dis 62:116–126
42. Ishigami J, Cowan LT, Demmer RT, Grams ME, Lutsey PL, Carrero J-J et al (2020) Incident hospitalization with major cardiovascular diseases and subsequent risk of ESKD: implications for cardiorenal syndrome. J Am Soc Nephrol 31:405–414
43. Park J, Wysocki RW, Amoozgar Z, Maiorino L, Fein MR, Jorns J et al (2016) Cancer cells induce metastasis-supporting neutrophil extracellular DNA traps. Sci Transl Med 8:361ra138

44. An Z, Li J, Jiangbo Yu, Wang X, Gao H, Zhang W et al (2019) Neutrophil extracellular traps induced by IL-8 aggravate atherosclerosis via activation NF-κB signaling in macrophages. Cell Cycle 18:2928–2938
45. Luyu Yang Lu, Liu RZ, Hong J, Wang Y, Wang J et al (2020) IL-8 mediates a positive loop connecting increased neutrophil extracellular traps (NETs) and colorectal cancer liver metastasis. J Cancer 11:4384–4396
46. Gao Q, Yang Y, Feng Y, Quan W, Luo Y, Wang H, Zheng J, Chen X, Huang Z, Chen X, Xu R, Zhang G, Gong L (2022) Effects of the NF-κB signaling pathway inhibitor BAY11-7082 in the replication of ASFV. Viruses 14(2):297
47. Dusza HM, Cenijn PH, Kamstra JH, Westerink RHS, Leonards PEG, Hamers T (2018) Effects of environmental pollutants on calcium release and uptake by rat cortical microsomes. Neurotoxicology 69:266–277. https://doi.org/10.1016/j.neuro.2018.07.015
48. Klein GL (2022) Is calcium a link between inflammatory bone resorption and heart disease? Elife 11:e83841. https://doi.org/10.7554/eLife.83841
49. Li S, Dong R, Kang Z, Li H, Wu X, Li T (2023) Exosomes: another intercellular lipometabolic communication mediators in digestive system neoplasms? Cytokine Growth Factor Rev 73:93–100. https://doi.org/10.1016/j.cytogfr.2023.06.005
50. Zhang X, Yu S, Li X, Wen X, Liu S, Zu R, Ren H, Li T, Yang C, Luo H (2023) Research progress on the interaction between oxidative stress and platelets: another avenue for cancer? Pharmacol Res 191:106777. https://doi.org/10.1016/j.phrs.2023.106777
51. Guo W, Qiao T, Li T (2022) The role of stem cells in small-cell lung cancer: evidence from chemoresistance to immunotherapy. Semin Cancer Biol 9(87):160–169. https://doi.org/10.1016/j.semcancer.2022.11.006
52. Li T, Qiao T (2022) Unraveling tumor microenvironment of small-cell lung cancer: Implications for immunotherapy. Semin Cancer Biol 86(Pt 2):117–125. https://doi.org/10.1016/j.semcancer.2022.09.005
53. Ma Z, Fan C, Yang Y, Di S, Hu W, Li T, Zhu Y, Han J, Xin Z, Wu G, Zhao J, Li X, Yan X (2016) Thapsigargin sensitizes human esophageal cancer to TRAIL-induced apoptosis via AMPK activation. Sci Rep 12(6):35196. https://doi.org/10.1038/srep35196
54. Li T, Yang Z, Jiang S, Di W, Ma Z, Hu W, Chen F, Reiter RJ, Yang Y (2018) Melatonin: does it have utility in the treatment of haematological neoplasms? Br J Pharmacol. 175(16):3251–3262. https://doi.org/10.1111/bph.13966
55. Yang Z, Jiang S, Lu C, Ji T, Yang W, Li T, Lv J, Hu W, Yang Y, Jin Z (2019) SOX11: friend or foe in tumor prevention and carcinogenesis? Ther Adv Med Oncol 3(11):1758835919853449. https://doi.org/10.1177/1758835919853449
56. Sun M, Liu X, Xia L, Chen Y, Kuang L, Gu X, Li T (2021) A nine-lncRNA signature predicts distant relapse-free survival of HER2-negative breast cancer patients receiving taxane and anthracycline-based neoadjuvant chemotherapy. Biochem Pharmacol 189:114285. https://doi.org/10.1016/j.bcp.2020.114285
57. Hu W, Yang Y, Fan C, Ma Z, Deng C, Li T, Lv J, Yao W, Gao J (2016) Clinical and pathological significance of N-Myc downstream-regulated gene 2 (NDRG2) in diverse human cancers. Apoptosis 21(6):675–682. https://doi.org/10.1007/s10495-016-1244-3
58. Wang L, Sun M, Yang S, Chen Y, Li T (2021) Intraoperative radiotherapy is not a better alternative to whole breast radiotherapy as a therapeutic option for early-stage breast cancer. Front Oncol 16(11):737982. https://doi.org/10.3389/fonc.2021.737982
59. Tomasello G, Mazzola M, Leone A et al (2016) Nutrition, oxidative stress and intestinal dysbiosis: influence of diet on gut microbiota in inflammatory bowel diseases. Biomed Pap Med Fac Univ Palacky Olomouc Czech Repub 160(4):461–466. https://doi.org/10.5507/bp.2016.052